Structures of low-lying states of a four-electron system in a quantum dot

Bao Chengguang
China Center for Advanced Science and Technology (World Laboratory), P.O. Box 8730, Beijing, 100080, People's Republic of China and Department of Physics, Zhongshan University, Guangzhou, People's Republic of China

Ruan Wenying and Liu Youyang
Department of Physics, South China University of Technology, Guangzhou, People's Republic of China

(Received 3 October 1995)

The methods for few-body systems are introduced to extract features of structure of low-lying states of a four-electron dot. Similarities among the states have been found, and accordingly a number of rotational bands have been identified. Each band is characterized by a specific mode of internal oscillation. The decisive effect of symmetry has been emphasized.

I. INTRODUCTION

Owing to the experimental creation of quantum dots,[1–3] the investigation of two-dimensional systems has become more attractive. A number of pioneering works have been done; important phenomena, e.g., the existence of magic angular momenta, have been discovered.[4–10] Since two-dimensional systems are relatively easier to control (e.g., the size and the number of electrons of a quantum dot) and to observe (e.g., the spatial distribution of the electrons), they are essential in developing microtechniques. They are also essential in the theoretical aspect, because rich information on microstructures can be extracted both theoretically and experimentally.

This paper is a continuation of Ref. 11 dedicated particularly to four-electron dots. The well-developed methods for three-dimensional few-body systems are specialized for use in two-dimensional systems. The features of structure and internal motion of the ground state and the low-lying excited states have been extracted. The aim is to arrive at a systematic understanding of the low-lying spectrum. Since we are interested in the global features of the dots but not the quantitative details, the emphasis is placed on the qualitative aspect. The role played by the quantum-mechanical (QM) symmetry is particularly emphasized.

The four electrons in a dot are subjected to a parabolic confinement. The Hamiltonian of this two-dimensional system is

$$H=\sum_{i=1}^{4}\left(\frac{P_i^2}{2m^*}+\frac{1}{2}m^*\omega_0^2 r_i^2\right)+\sum_{i>j}\frac{e^2}{4\pi\varepsilon r_{ij}}, \tag{1}$$

where $\mathbf{r}_i$ is the position vector of the ith electron (e_i) originated from the center of the dot, m^* is the effective mass, $r_{ij}=|\mathbf{r}_i-\mathbf{r}_j|$. The center-of-mass coordinates and the internal coordinates are then introduced. Then

$$H=H_{\text{c.m.}}+H_I, \tag{2}$$

where $H_{\text{c.m.}}$ is for the motion of the center of mass, H_I is for internal motions. Let $\mathbf{r}_{12}$, $\mathbf{r}_{34}$, $\mathbf{R}$ be chosen as a set of internal coordinates (shown in Fig. 1), then

$$H_I=\frac{p_{12}^2}{2\mu_{12}}+\frac{p_{34}^2}{2\mu_{34}}+\frac{p_R^2}{2\mu_R}+\mathbb{V}, \tag{3}$$

$$\mathbb{V}=\sum_{i>j}U(r_{ij}),$$

where $\mu_{12}=m^*/2$, $\mu_{34}=m^*/2$, $\mu_R=m^*$; $\mathbb{V}$ is the total potential energy, $U(r_{ij})$ is the equivalent pairwise interaction,

$$U(r_{ij})=\tfrac{1}{8}m^*w_0^2r_{ij}^2+e^2/(4\pi\varepsilon r_{ij}), \tag{4}$$

which is attractive at large separation (due to the parabolic confinement) but repulsive at small separation (due to Coulomb force); thereby there is a minimum at $r_0=(e^2/\pi\varepsilon m^* w_0^2)^{1/3}$. Owing to the minimum, as we shall see, the system would pursue an optimal shape and size to optimize the binding energy.

Since the motion of the center of mass is trivial (simply a harmonic oscillation), only the internal structure is discussed. To obtain the eigenenergies and eigenstates, H_I is diagonalized in a model space spanned by a set of basis functions with a total orbital angular momentum L and a total spin S as

$$\tilde{\phi}_i=\mathscr{A}\{\varphi_{n_a l_a}^w(\mathbf{r}_{12})\varphi_{n_b l_b}^w(\mathbf{r}_{34})\varphi_{n_c l_c}^w(R)\chi_{s_1 s_2}^S\}, \tag{5}$$

where φ_{nl}^w is a two-dimensional harmonic oscillator state with a frequency w, an energy $(2n+l+1)\hbar w$, and an orbital angular momentum l;[12] $l_a+l_b+l_c=L$ is assumed; $\chi_{s_1 s_2}^S$ is the spin part, where the spins of e_1 and e_2 are coupled to s_1, e_3 and e_4 to s_2, and s_1 and s_2 are coupled to S. When $w=w_0$, the basis function is an exact solution of H_I if the Coulomb repulsion is removed. In practice, w serves as a variational parameter around w_0 to minimize the eigenenergies. $\mathscr{A}$ is an antisymmetrizer. The antisymmetrization and the calculation of related matrix elements are realized by using two-dimensional Talmi-Moshinsky coefficients.[12–14] It is notable that the basis functions do not form an orthogonal set due to the antisymmetrization; hence, in practical calculation, an additional procedure of orthogonalization is needed to extract linearly independent basis functions.

The accuracy of the solutions depends on how large the model space is. Since we are interested only in the low-lying

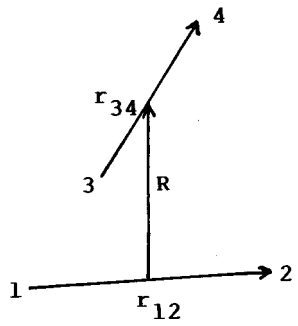

FIG. 1. The internal coordinates.

states and in the qualitative aspect, the model space adopted is neither very large to facilitate numerical calculation, nor very small to assure the qualitative accuracy. This is achieved by extending the dimension of the model space step by step; in each step the new results are compared with the previous results from a smaller space, until satisfactory convergence is achieved. For example, when $L=6$ and $S=2$, model spaces of 15, 37, and 76 dimensions have been used, stopping finally at 76. In what follows the energies are in meV, and the lengths are in $a_0=\sqrt{\hbar/m^*w_0}$; $hw_0=0.01$, $m^*=0.067m_e$, and $\varepsilon=13.1$ are adopted in the calculation.

II. THE ENERGY SPECTRUM AND THE EFFECT OF SYMMETRY

Let the states be denoted as $^{2S+1}L(i)$, $i=1,2,...$ where the $i=1$ state is the lowest of the series, which is named a head state; the $i=2$ state is named a second state. The energy spectrum of low-lying states with $L\leqslant 6$ is given in Fig. 2. It has the following features: (i) In $S=0$ states, the head states with L even are remarkably lower than the head states with L odd. (ii) In $S=1$ states, the head states with $L=2$ or 6 are remarkably higher than the other head states. (iii) In $S=2$ states, the head states with $L=2$ or 6 are remarkably lower than the other head states. (iv) In the above three cases, the groups of head states with remarkably low energies are mutually close in energy. Besides, in these states, the energy gap between the head and second state is particularly big.

The above features have a profound background of symmetry. If the particles form a square (SQ) with an optimal side length (close to r_0), then the potential energy is minimized. However, the SQ may be prohibited by symmetry. Let the eigen-wave-function of H_I be written as

$$\Psi=\sum_i c_i\tilde{\phi}_i=\sum_{s_1s_2}\psi_L^{s_1s_2}(1234)\chi^S_{s_1s_2}. \tag{6}$$

If the particles form a SQ, then a rotation about the c.m. by $\pm 90°$ is equivalent to a cyclic permutation of the particles. Thus at a square we have

$$e^{i(\pi/2)L}\psi_L^{s_1s_2}(1234)=\psi_2^{s_1s_2}(2341). \tag{7}$$

On the other hand, since Ψ is antisymmetrized, from the representation theory of the symmetric group, when $S=0$ we have

$$\begin{aligned}\psi_L^{00}(2341)&=-\tfrac{1}{2}\psi_L^{00}(1234)+\sqrt{3}/2\psi_L^{11}(1234),\\ \psi_L^{11}(2341)&=\sqrt{3}/2\psi_L^{00}(1234)+\tfrac{1}{2}\psi_L^{11}(1234).\end{aligned} \tag{8a}$$

When $S=1$, we have

$$\begin{aligned}\psi_L^{01}(2341)&=\tfrac{1}{2}\psi_L^{01}(1234)+\tfrac{1}{2}\psi_L^{10}(1234)-\sqrt{1/2}\psi_L^{11}(1234),\\ \psi_L^{10}(2341)&=\tfrac{1}{2}\psi_L^{01}(1234)+\tfrac{1}{2}\psi_L^{10}(1234)+\sqrt{1/2}\psi_L^{11}(1234),\\ \psi_L^{11}(2341)&=\sqrt{1/2}\psi_L^{01}(1234)-\sqrt{1/2}\psi_L^{10}(1234).\end{aligned} \tag{8b}$$

When $S=2$, we have

$$\psi_L^{11}(2341)=-\psi_L^{11}(1234). \tag{8c}$$

Combining (7) and (8), when the particles form a SQ, the following sets of homogeneous linear equations hold:

$$\begin{pmatrix} e^{i(\pi/2)L}+1/2 & -\sqrt{3}/2 \\ -\sqrt{3}/2 & e^{i(\pi/2)L}-1/2 \end{pmatrix}\begin{matrix}\psi_L^{00}(\mathrm{SQ})\\ \psi_L^{11}(\mathrm{SQ})\end{matrix}=0 \quad (\text{if } S=0), \tag{9a}$$

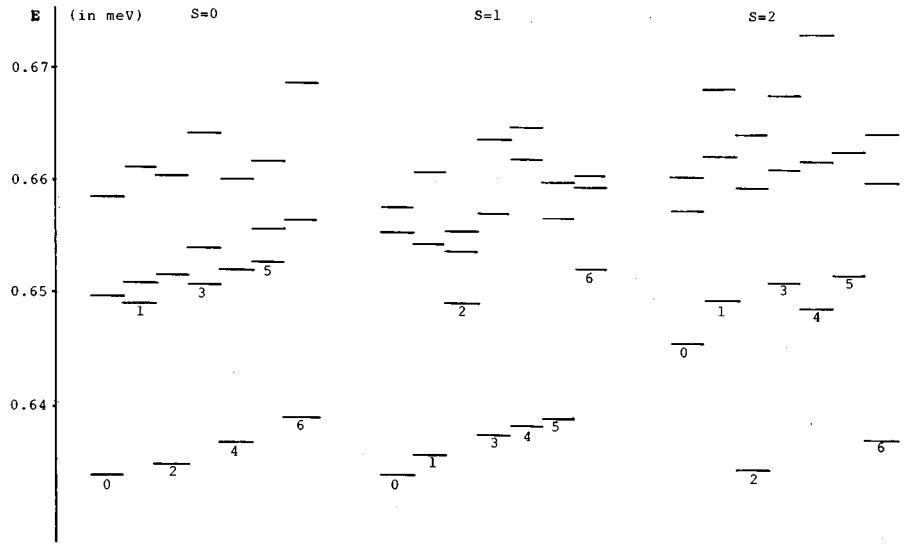

FIG. 2. Low-lying energy spectrum (in meV) of $S=0$ (at the left), $S=1$ (middle), and $S=2$ (right) states. The levels in each column have the same L (marked under the head states).

$$\begin{pmatrix} e^{i(\pi/2)L}-1/2 & -1/2 & \sqrt{1/2} \\ -1/2 & e^{i(\pi/2)L}-1/2 & -\sqrt{1/2} \\ -\sqrt{1/2} & \sqrt{1/2} & e^{i(\pi/2)L} \end{pmatrix} \begin{matrix} \psi_L^{01}(\mathrm{SQ}) \\ \psi_L^{10}(\mathrm{SQ}) \\ \psi_L^{11}(\mathrm{SQ}) \end{matrix} = 0$$

$$(\text{if } S=1), \quad (9b)$$

$$(e^{i(\pi/2)L}+1)\psi_L^{11}(\mathrm{SQ})=0 \quad (\text{if } S=2), \quad (9c)$$

where the notation SQ denotes that the particles form a SQ. In Eq. (9), nonzero solutions exist only if the determinants are zero; i.e., only if the following equations are fulfilled:

$$(e^{i\pi L}-1)=0 \quad (\text{if } S=0),$$

$$(e^{i\pi L}+1)(e^{i(\pi/2)L}-1)=0 \quad (\text{if } S=1), \quad (10)$$

$$(e^{i(\pi/2)L}+1)=0 \quad (\text{if } S=2).$$

It implies that a state is nonzero at SQ only if L is even (if $S=0$), or $L\neq 4n+2$ (if $S=1$, where $n=0,1,2,...$), or $L=4n+2,...$ (if $S=2$). If it does, it is called a ''SQ-accessible state.'' Alternatively, in a SQ-inaccessible state, a nodal surface exists at SQ configurations. This surface is originated purely from symmetry, it is named an inherent nodal surface (INS), which was found to be decisive to the structures of few-body systems.[11,15–17,19]

Now the main features of the spectrum can be easily explained, where all the SQ-accessible head states are remarkably lower. In these head states, the wave function is smoothly distributed around a SQ without nodal surface. In this way the potential energy can be optimized and the internal excitation is avoided (the furiousness of an internal excitation is measured by the number of nodal surfaces contained in the wave function). Besides, since these states have similar internal structures, they are close in energy as shown in Fig. 2 (in our model, the energy for collective rotation is small). Furthermore, since the structures of these states are very stable, they should be harder to excite, resulting in a larger energy gap.

III. THE SHAPE DENSITY

In order to have a systematic understanding of the spectrum, let us analyze the wave functions in detail. When the system is subjected to a strong magnetic field, the spins of electrons will be aligned and accordingly the spatial wave function is totally antisymmetric. This is just the case of $S=2$. Hence, the case of $S=2$ is more important than the $S=0$ and $S=1$ cases. For this reason, we shall mainly discuss the $S=2$ case. In what follows the discussions are limited to the $S=2$ and $L\leqslant 6$ cases except in the last section.

It is well known that the size of a few-body system can be evaluated in terms of the hyper-radius. Hence, let us introduce the hypercoordinates,[18] which are defined from the internal coordinates as

$$\begin{aligned} \xi &= [(\mu_{12}r_{12}^2+\mu_{34}r_{34}^2+\mu_R R^2)/m^*]^{1/2}, \\ \sqrt{\mu_R/m^*}R &= \xi\cos\alpha, \\ \sqrt{\mu_{12}/m^*}r_{12} &= \xi\sin\alpha\cos\beta, \\ \sqrt{\mu_{34}/m^*}r_{34} &= \xi\sin\alpha\sin\beta, \end{aligned} \quad (11)$$

where ξ is the hyper-radius specifying the size; α and β are hyperangles, together with $\hat{r}_{12}$, $\hat{r}_{34}$, and $\hat{R}$, specifying the shape and its orientation (we shall neglect the discussion on orientation, because the density is irrelevant to it). It is noticed that the weighted distances $\sqrt{\mu_R/m^*}R$,... are used in Eq. (11) to assure the invariance of ξ under transformations of different sets of internal coordinates.

Let ψ_L^{11} be rewritten as ψ_L, and $^{2S+1}L(i)$ as $L(i)$. Using the hypercoordinates, the equation of normalization is written as

$$1=\int d\xi\, d\mathbb{S}\, J|\psi_L|^2, \quad (12)$$

where $d\xi$ is an infinitesimal variation of size, $d\mathbb{S}=d\alpha\, d\beta\, d\hat{r}_{12}d\hat{r}_{34}d\hat{R}$ is an infinitesimal variation of shape, J arises from the transformation of arguments,

$$J=\xi^5\cos\alpha\sin^3\alpha\cos\beta\sin\beta\frac{m^{*3}}{\mu_{12}\mu_{34}\mu_R}. \quad (13)$$

From Eq. (12), it is clear that $J|\psi_L|^2$ is the probability density of the system at a given size, orientation, and shape. However, in practice, the measurement should be blind to the permutation of particles. Hence, the shape density is formally defined as

$$\mathscr{S}_S=\frac{1}{N!}\sum_p J|\psi_L|^2=\left(\frac{1}{N!}\sum_p J\right)|\psi_L|^2, \quad (14)$$

where the summation runs over all the permutations, and N is the number of particles. In $\mathscr{S}_S$, the physics is contained in $|\psi_L|^2$, J is simply a factor of modification arising from geometry.

Let the maximum of $\mathscr{S}_S$ be denoted by $\mathscr{S}_S^M$; the shape where $\mathscr{S}_S$ arrives at $\mathscr{S}_S^M$ is named a preferred shape. Among the preferred shapes, the one with the largest $\mathscr{S}_S^M$ is named a most probable shape. It was found that the wave functions are usually distributed sharply around the preferred shapes (as shown later), hence the geometric feature can be demonstrated by the preferred shapes.

The preferred shapes for $S=2$ states are listed in the second column of Table I; the associated $\mathscr{S}_S^M$ are listed in the third column. For each preferred shape characteristic lengths are defined in Fig. 3 and are given in the fourth column.

It was shown in Table I that some states [e.g., the 2(1) state] have only one preferred shape, and thereby dominated by one kind of geometric structure. In other states, different geometric structures coexist [e.g., in the 1(1) state]. It was found that some states are surprisingly very similar to each other both in shape and in size. For example, the 0(1) and 4(1) states are similar; 2(1) and 6(1) are similar; 1(1), 3(1), and 5(1) are similar; and so on. The detailed features of the low-lying states will be discussed as follows.

TABLE I. The preferred shapes. CET denotes the centered-equilateral triangle. The characteristic lengths are referred to Fig. 3.

$L(i)$ state	Preferred shapes	Maximal values of the shape density	Characteristic lengths
0(1)	Diamond	2.29	$d_1=5.0,\ d_2=7.8$
0(2)	Rectangle	2.10	$h=3.8,\ s=5.7$
0(3)	CET	3.20	$h=3.8$
1(1)	Shield	1.93	$d=7.2,\ h_1=1.5,\ h_2=4.5$
	Trapezoid	1.46	$w=4.6,\ s_1=3.5,\ s_2=6.3$
2(1)	Square	4.62	$s=4.63$
2(2)	Shield	1.45	$d=8.1,\ h_1=0.3,\ h_2=3.9$
	Square	0.80	$s=4.95$
2(3)	Square (smaller)	2.01	$s=3.82$
	Square (larger)	1.73	$s=5.50$
3(1)	Shield	1.78	$d=7.3,\ h_1=1.3,\ h_2=4.3$
	Trapezoid	1.06	$w=4.7,\ s_1=3.6,\ s_2=6.4$
3(2)	CET	2.98	$h=3.9$
3(3)	CET	2.98	$h=4.0$
4(1)	Diamond	2.08	$d_1=5.0,\ d_2=7.8$
4(2)	Rectangle	1.56	$h=3.8,\ s=5.7$
5(1)	Shield	1.75	$d=7.1,\ h_1=1.5,\ h_2=4.5$
	Trapezoid	1.65	$w=4.7,\ s_1=3.5,\ s_2=6.3$
6(1)	Square	4.57	$s=4.64$
6(2)	Shield	1.60	$d=7.9,\ h_1=-0.4,\ h_2=4.6$
	Square	0.85	$s=4.95$
	CET	1.36	$h=3.9$
6(3)	CET	1.90	$h=4.0$
	Diamond	1.49	$d_1=4.1,\ d_2=8.2$

IV. THE HEAD STATES ($S=2$)

A. The SQ states 2(1) and 6(1)

We have pointed out in Sec. III that the $L=2$ and 6 states are SQ accessible. From Table I it is confirmed that the 2(1) and 6(1) are dominated by the SQ structure; they are named SQ states. Let $\mathscr{S}_S$ be observed in the subspace of SQ as shown in Fig. 4. It is obvious that in this subspace $\mathscr{S}_S$ is nonzero only if $L=2$ or 6. The curves for 2(1) and 6(1) in Fig. 4 are remarkably sharp; these two curves are nearly identical. Thus the SQ structure is well defined and the similarity of these two states is explicit. The curves for 2(3) contain two peaks, thus it is a coexistence of a small SQ and a large SQ. The peaks in the curves for 2(2), 6(2), and 6(3) are lower; these states are coexistences of a SQ and other shapes.

Evidently, all the SQ-accessible head states would do their best to pursue the SQ structure to lower their energy. Hence, not only the 2(1) and 6(1), but all the head states with $L=2+4n$ would have the same SQ structure; accordingly they form a very stable (much lower in energy) rotational band

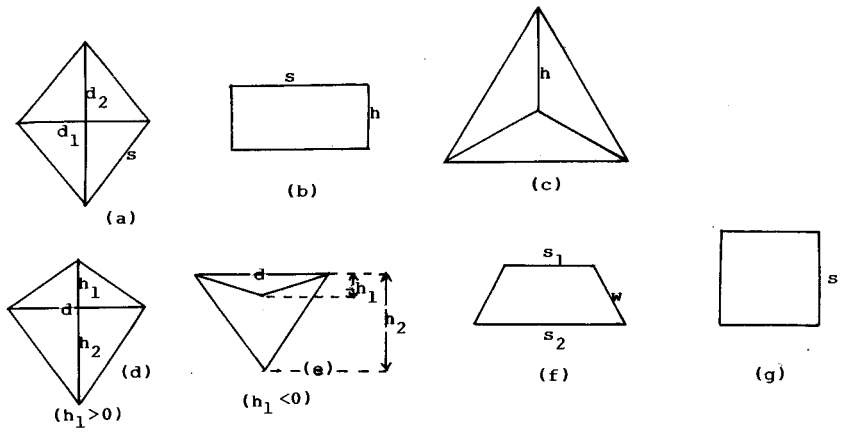

FIG. 3. The preferred shapes found in $S=2$ states, where characteristic lengths are labeled. (c) and (e) are centered structures.

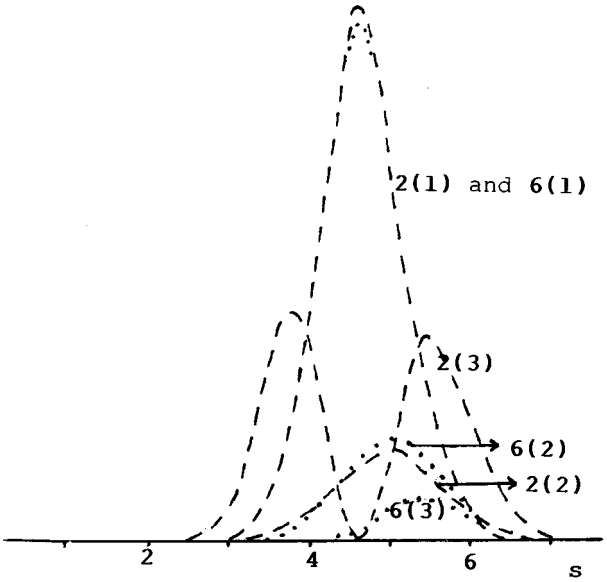

FIG. 4. $\mathscr{S}_S$ as a function of the side length s of a square. $r_{12}=r_{34}=R=s$ and $\mathbf{r}_{12}\|\mathbf{r}_{34}$, $\mathbf{r}_{12}\perp\mathbf{R}$ are assumed. The ordinate is in arbitrary unit. A dashed line is for $L=2$ and dotted line for $L=6$ states.

(the SQ band). This explains the well-known magic angular momenta 2,6,10,... in spin-aligned four-electron dots.[4–7,11]

B. The diamond states 0(1) and 4(1)

In a SQ, the bond of a side is stronger than the bond of a diagonal. Hence, if a SQ is changed to a diamond with the lengths of the side being unchanged, the energy increase is small because only the two weaker bonds of the diagonals are concerned. For this reason, the diamond shape will be the first choice of SQ-inaccessible head states. For a diamond, a rotation by 180° is equivalent to two interchanges of particles; the former operation induces an factor $e^{i\pi L}$, while the latter causes no change in $S=2$ states. Thus we have

$$(1-e^{i\pi L})\psi_L(\mathrm{DIA})=0, \tag{15}$$

where the label DIA denotes the diamond. Equation (15) tells us that ψ_L (DIA) is nonzero only if L is even. Hence, among the SQ-inaccessible states, only the $L=4n$ states are DIA accessible.

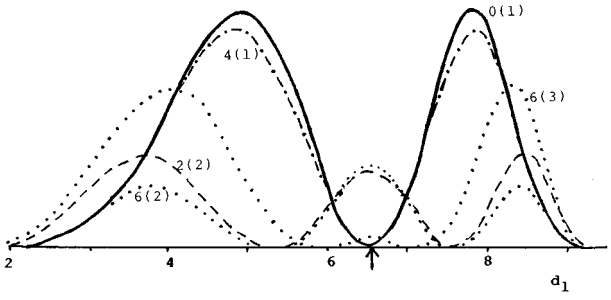

FIG. 5. $\mathscr{S}_S$ as a function of the diagonal d_1 of diamonds. The other diagonal d_2 is constrained by $(d_1/2)^2+(d_2/2)^2=s^2$. s is the side length of the diamonds fixed at an optimal value 4.63. The vertical arrow designates a square ($d_1=d_2=\sqrt{2}s$). A solid line is for $L=0$, dashed line for $L=2$, dash-dot line for $L=4$, and dotted line for $L=6$ states.

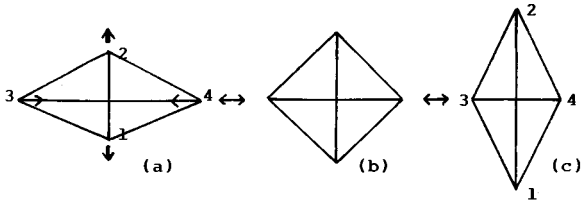

FIG. 6. An intuitive picture of the diamond-SQ-diamond (D-SQ-D) mode of oscillation.

From the above analysis, the 0(1) and 4(1) are expected to have the diamond structure. This is true as shown in Table I. Furthermore, let $\mathscr{S}_S$ be plotted in the subspace of diamonds with the side length being fixed as shown in Fig. 5 [where the curves for 2(1) and 6(1) have been omitted]. This figure shows us that the curves for 0(1) and 4(1) are remarkably higher and similar to each other. Thus both states are dominated by the diamond and have similar internal structures. Incidentally, the $\mathscr{S}_S$ of higher $L=0$ and 4 states are too small to be seen in Fig. 5; thus the diamond is not preferred by these excited states.

The diamond is not a stable configuration. If a diamond is transformed to a SQ, $\mathbb{V}$ would be lower. In classical mechanics, there is a periodic oscillation as shown in Fig. 6, where the increase of length of a diagonal matches the decrease of another diagonal so that a flattened diamond is changed to a SQ, and then to a sharpened diamond, and vice versa. This is named a diamond-SQ-diamond (D-SQ-D) oscillation. In our QM system, let $\mathscr{S}_S$ be observed in the subspace of diamonds as a function of d_1 and d_2 plotted in Fig. 7. In Fig. 7(a), the point A is associated with Fig. 6(a), B with 6(b), and C with 6(c). Since the configuration shown in 6(a) can be changed to 6(c) via a rotation by 90° together with a cyclic permutation of the particles, the former causes no effect in $L=4n$ states, while the latter causes a change in sign in $S=2$ states. Hence the wave functions at A and C must have opposite signs. The point B (a SQ) is a node for $L=4n$ states due to being SQ inaccessible. Thus, along A-B-C, the wave function varies from a peak to an antipeak via a node; it is similar to a linear harmonic oscillator with one quantum of excitation. Hence, the 0(1) state contains the D-SQ-D mode of oscillation with one node.

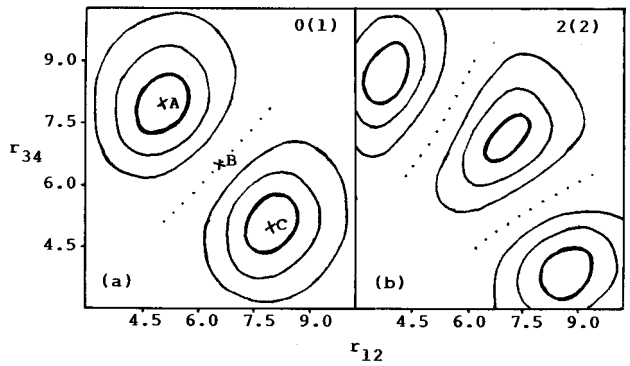

FIG. 7. $\mathscr{S}_S$ as a function of r_{12} and r_{34}. $R=0$ and $\mathbf{r}_{12}\perp\mathbf{r}_{34}$ are assumed, thus r_{12} and r_{34} are the diagonals of a diamond. The contours give 20%, 50%, and 80% of the maximum in each figure. The dotted line is a nodal line.

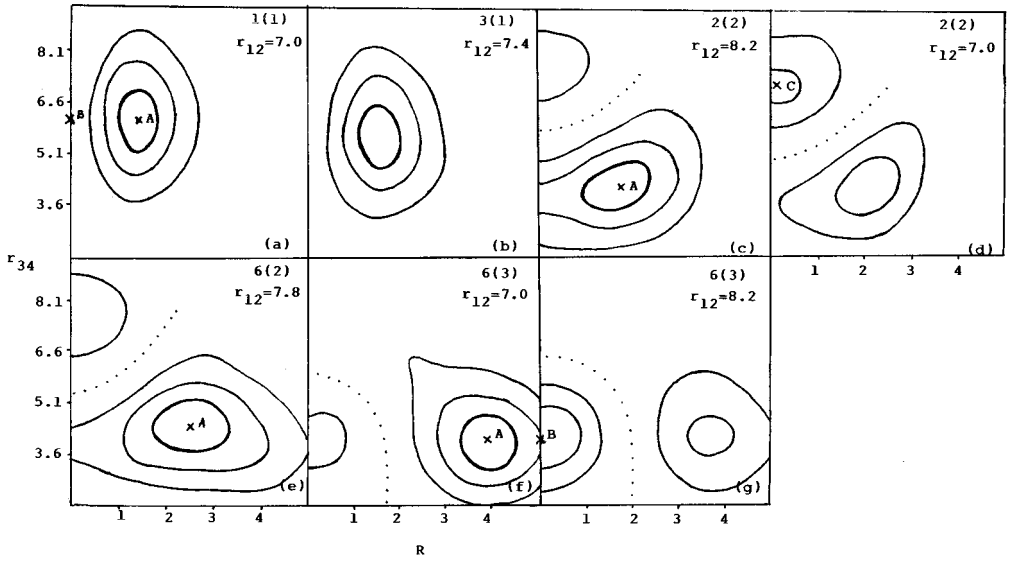

FIG. 8. $\mathscr{S}_S$ as a function of R and r_{34} with r_{12} given at a specified value. $\mathbf{r}_{12}\perp\mathbf{r}_{34}$ and $\mathbf{R}\|\mathbf{r}_{34}$ are assumed. Refer to the caption of Fig. 7. When a pair of subfigures belong to the same state [(c) and (d), (f) and (g)], the larger maximum of the pair is used as the scale for the contours.

If Fig. 7(a) is replotted for the 4(1) state, the contour diagram is changed scarcely. This is expected to be true for other $L=4n$ head states with a larger L. Thus, the second rotational band based on D-SQ-D oscillation is suggested. Since one quantum of internal excitation is contained in the D-SQ-D band, it should be explicitly higher than the SQ band as shown in Fig. 2.

C. L odd states

Let the regular shapes be divided into two types. The first type is invariant under a space inversion (with respect to the c.m.), while the second type is not. Evidently, the first type is better in geometric symmetry; it contains the SQ, the rectangle, the diamond, and the parallelogram. The second type contains the shield [Fig. 3(d)] and the trapezoid [Fig. 3(f)]. Let one particle be put at each vertex; then in the first type a space inversion is equivalent to two interchanges of particles. The former provides a factor π (parity), while the latter causes no change in $S=2$ states. Hence, only even-parity states (i.e., L even) are allowed to pursue the first type, all the odd-parity states (i.e., L odd) can only pursue the second type. In fact, it is shown in Table I that all the 1(1), 3(1), and 5(1) states are a coexistence of a shield and a trapezoid.

Let the shape density be plotted in the subspace of shields. In Fig. 8(a), r_{12} serves as the horizontal diagonal in Fig. 3(d), which is given at an optimal value, r_{34} serves as the vertical diagonal. There is a peak at A associated with Fig. 9(a). Let C be the partner point of A arising from $\mathbf{R}\rightarrow-\mathbf{R}$, then it is associated with Fig. 9(c). There should also be a peak at C, because Fig. 8 is unchanged under $\mathbf{R}\rightarrow-\mathbf{R}$. The point B at $R=0$ is associated with a diamond [Fig. 9(b)]; thus B is a node for L odd states. The wave functions at A and C have opposite signs (due to the QM symmetry). Thus, an evolution along A-B-C implies an oscillation (associated with the variation of R) with one node, and accordingly an up-shield [Fig. 9(a)] is changed to a down-shield [9(c)] via a diamond, and vice versa. It is named a SH-D-SH mode; in this mode, the two particles at the top and bottom of a diamond shift as a whole upward and downward repeatedly.

Similarly, by observing $\mathscr{S}_S$ in the subspace of trapezoids, a mode of oscillation is found around the trapezoid as shown in Fig. 10, where an up-trapezoid is transformed to a down-trapezoid via a SQ. It is named a TR-SQ-TR mode; in this mode, the extension of the upper side of a trapezoid matches the contraction of the lower side, and vice versa.

It was found that the features of the 3(1) and 5(1) states are very similar to the 1(1) state. For example, Fig. 8(b) is for the 3(1) state, which is very similar to 8(a). This is natural because they are constrained in the same way by the QM symmetry. Thus the third rotational band composed of all the $L=2n+1$ head states based on a coupling of the SH-D-SH mode and the TR-SQ-TR mode is suggested. Although both the L odd band and the D-SQ-D band contain one node in

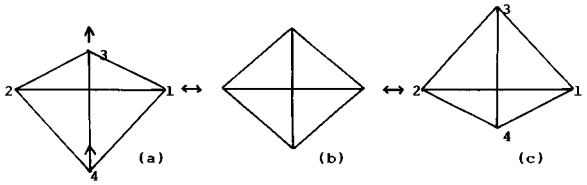

FIG. 9. The shield-diamond-shield (SH-D-SH) mode of oscillation.

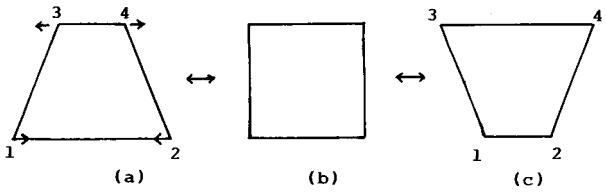

FIG. 10. The trapezoid-SQ-trapezoid (TR-SQ-TR) mode.

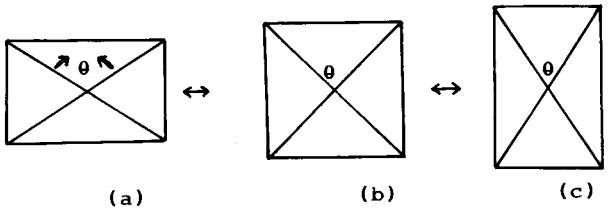

FIG. 11. The rectangle-SQ-rectangle (REC-SQ-REC) mode.

their internal oscillations, however, the former is less symmetric in shape, resulting in having a higher energy as shown in Fig. 2.

All the head states are well divided into three rotational bands according to $L=4n+2$, $4n$, and $2n+1$. These bands are based on a SQ, a diamond, and a coexistence of a shield and a trapezoid, respectively. The first band does not contain internal excitation (without nodal surface), while the other two contain one quantum of internal excitation (with a nodal surface). How the states are classified into these bands is determined by the QM symmetry, and not by the dynamical parameters adopted.

V. THE STATES HIGHER THAN THE HEAD STATES ($S=2$)

We are not going into a comprehensive discussion; instead, certain higher states are selected to reveal specific modes of excitation.

A. The rectangle states 0(2) and 4(2)

A SQ can be varied in different ways with the inversion-invariance remained. One is a variation of the lengths of the diagonals leading to a diamond (as shown in Fig. 6); one is a variation of the angle θ between the two diagonals leading to a rectangle (as shown in Fig. 11). Now the diamond has already been adopted by the 0(1),4(1),... states. It is natural to think that the rectangle may be adopted by the 0(2),4(2),... states.

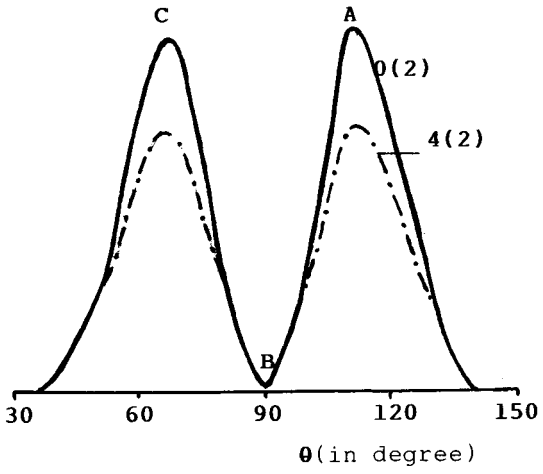

FIG. 12. $\mathscr{S}_S$ as a function of θ (marked in Fig. 11) in the subspace of rectangles. $r_{12}=r_{34}=7.83$ and $R=0$ are assumed. The solid line is for $L=0$, the dash-dotted line is for $L=4$ states.

It is shown in Table I that the most probable shapes of the 0(2) and 4(2) states are rectangles. In Fig. 12, $\mathscr{S}_S$ of all the $L=2$ and 4, $i=1$–3 states are plotted in the subspace of rectangles as a function of θ. There are two peaks at A and C associated with Figs. 11(a) and 11(c), respectively. The point B at $\theta=90°$ is associated with a SQ and is a node for $L=4n$ states. The wave functions at A and C have opposite signs [due to the QM symmetry; in detail, Fig. 11(a) can be changed to 11(c) via a rotation by 90° together with a cyclic permutation of particles]. The evolution from A to C implies an oscillation as shown in Fig. 11. It is named a REC-SQ-REC mode. Figure 12 shows that the curves for the 0(2) and 4(2) states are similar, while the curves for the other states are too small to be seen. It is suggested that the 0(2) and 4(2) states are the lowest members of a rectangle band characterized by the REC-SQ-REC mode.

B. Single-particle oscillation and 2(2) and 6(2) states

It has been stated that the 2(1) state is a SQ state. One may naturally think that the 2(2) state may be dominated by an inversion-invariant excitation, in particular by the D-SQ-D mode. However, this is not true. Table I tells us that the 2(2) state is a coexistence of a shield and a SQ, the former is more important. This arises because, in the D-SQ-D mode, the wave functions at the two configurations associated with Figs. 6(a) and 6(c) have the same sign in $S=2$ and $L=2$ states (due to the QM symmetry). It implies that at least two nodes would be contained if the D-SQ-D mode is adopted. Hence, the D-SQ-D mode is not very advantageous.

Since the most probable shape of the 2(2) state is a shield, let $\mathscr{S}_S$ of 2(2) be observed in the subspace of shields as shown in Figs. 8(c) ($r_{12}=8.2$) and 8(d) ($r_{12}=7.0$). Where point A in 8(c) is associated with the shape in the solid line in Fig. 13(a), point C in Fig. 8(d) is associated with the SQ in the dotted line in Fig. 13(a). There is a nodal surface lying between A and C; this surface is not originated from the QM symmetry but from a pure dynamical background.[15] It induces an evolution from A to C, and back to A, which is essentially an oscillation of one particle relative to the other three as shown in Fig. 13(a). Hence, it is named a single-particle mode. Incidentally, the D-SQ-D mode with two nodes is also found in the 2(2) state as shown in Fig. 5 and in Fig. 7(b). However, the $\mathscr{S}_S$ at the SQ is only 0.80, much smaller than 1.45 of the shield. Hence, the D-SQ-D mode is not the main mode while the single-particle mode is. Since at

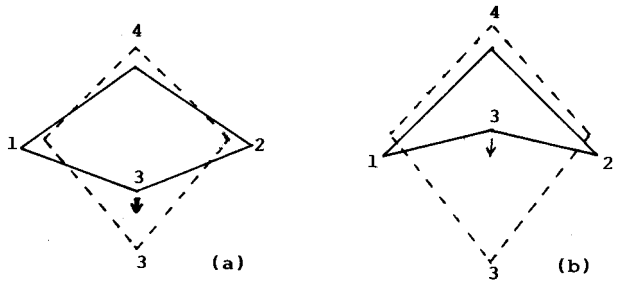

FIG. 13. An intuitive picture to show the single-particle oscillation.

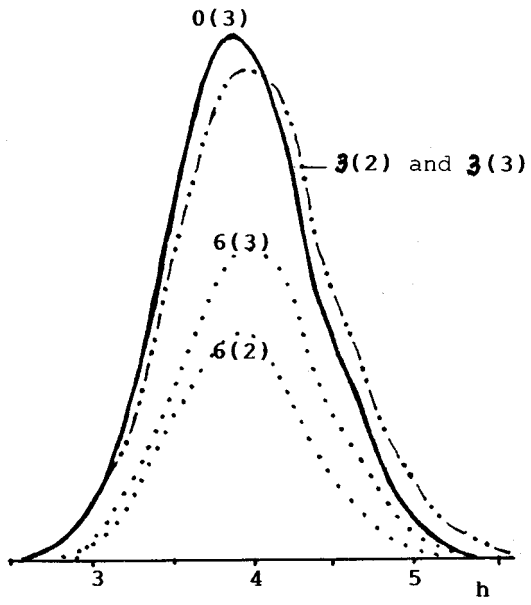

FIG. 14. $\mathscr{S}_S$ as a function of h [marked in Fig. 3(c)] in the subspace of CET.

least three bonds are involved in the single-particle mode, this mode is energetic, resulting in a big gap between the second state and the head state.

The 6(2) state is found to be also dominated by the single-particle mode as shown in Fig. 8(e). Besides, the D-SQ-D mode with two nodes is also contained in 6(2). Thus, 6(2) is similar to 2(2). However, the peak at A in Fig. 8(e) is more shifted to the right, thus it is associated with a centered triangle shown by the solid lines in Fig. 13(b). Hence, the amplitude of the single-particle mode in 6(2) is larger than the one in 2(2). The 2(2),6(2),10(2),... states are suggested to form a rotational band mainly based on the single-particle mode.

C. The centered equilateral triangle (CET) states

The CET [Fig. 3(c)] has good geometric symmetry. However, in this shape only three bonds can be optimized. Hence, it is less advantageous in binding. Nonetheless, in higher states, this shape will compete with other shapes. When the particles form a CET, a rotation by 120° is equivalent to a cyclic permutation of three particles. The former induces a $e^{i(2\pi/3)L}$ factor in the wave function, while the latter causes no effect in $S=2$ states, thus we have[11,19]

$$(1-e^{i(2\pi/3)L})\psi_L(\mathrm{CET})=0. \tag{16}$$

Equation (16) implies that CET is allowed only in $L=3n$ states. In fact, it is shown in Table I that the CET states do emerge in higher $L=0$, 3, and 6 states.

Let the $\mathscr{S}_S$ be plotted in the subspace of CET as shown in Fig. 14. It is shown that, among all $L\leqslant 6$, $S=2$, and $i\leqslant 3$ states, there are four states, i.e., the 0(3), 3(2), 3(3), and 6(3), dominated by this structure; they also have similar size. In the 6(2) state the CET is less important than a shield (with a negative h_1); both in the CET or in the shield one particle has penetrated into the interior of the other three due to the large-amplitude single-particle oscillation. It is noticeable

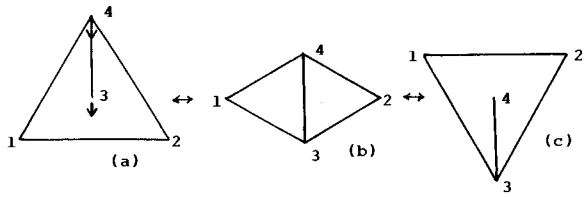

FIG. 15. A large-amplitude oscillation transforming an up CET to a down CET.

that the CET is more favorable in the $L=3$ states than in the $L=0$ or 6 states. In the former, the CET competes with inversion-variant shapes: thus it can emerge in the second state. In the latter, it has to compete with the SQ (if $L=6$), or the diamond (if $L=0$), thereby it has more difficulty emerging.

A strong oscillation was found in the 3(2), 3(3), and 6(3) states as shown in Fig. 15, where an up CET is transformed to a down CET via a diamond, and vice versa. For example, $\mathscr{S}_S$ of the 6(3) state are plotted in Figs. 8(f) and 8(g) with $r_{12}=7.0$ and 8.2, respectively. Point A in Fig. 8(f) is associated with the CET in Fig. 15(a); point B in 8(g) is associated with the diamond in 15(b). There is a nodal surface lying between A and B. The evolution from A to B implies an increase of r_{12} and a decrease of R, so that particles 1 and 2 [Fig. 15(a)] move outward and 3 and 4 move downward; accordingly, the up CET is transformed to the diamond (the diamond is lower in potential energy). Then, the pair 3 and 4 keeps going down, and the diamond is transformed to a down CET, and vice versa. This is named a CET-D-CET mode.

D. The breathing mode

It was well known that the breathing mode (extension and contraction of size) exists in three-dimensional systems. For example, it was named a monopole excitation in nuclear theory.[20] Now, this mode is found in the 2(3) state as shown in Table I and Fig. 4; it reveals that the monopole excitation exists also in two-dimensional systems. Since all bonds are involved in breathing, this mode is energetic, thereby it appears only in high excited states. There may be a rotational band based on breathing modes. However, since only a shape with good geometric symmetry can be stable enough to be free from deformation during an energetic oscillation, the breathing is likely to occur only in SQ states. Hence, the candidates of this band will be the 2(3),6(4) or 6(5),10(3),...; this suggestion is left to be checked.

VI. FINAL REMARKS

(1) Each state has its own feature of geometric structure and internal motion. When the wave function is smoothly distributed around a most probable shape, it is recognized as a small oscillation around this shape as an equilibrium shape, e.g., a SQ in the 2(1) state. When the wave function contains nodal surfaces, the internal motion becomes energetic. There are two types of nodal surfaces.[15] One arises purely from the constraints of the QM symmetry, the other one arises simply from dynamics without symmetry background. The first type

TABLE II. The rotational bands.

Feature of internal oscillation	The states contained in the band	Number of nodes in oscillation
A small oscillation around a SQ	2(1),6(1),10(1),...	0
Breathing of a SQ	2(3),6(4) or 6(5),10(3),...	1
D-SQ-D mode	0(1),4(1),8(1),...	1
SH-D-SH mode+TR-SQ-TR mode	1(1),3(1),5(1),...	1
REC-SQ-REC mode	0(2),4(2),8(2),...	1
Single-particle oscillation	2(2),6(2),...	1
A small oscillation around a CET	0(3),...	0
CET-D-CET mode	3(2),3(3),6(3),...	$\geqslant 2$

(INS) is particularly important because it usually locates at configurations with good geometric symmetry, and thus with lower potential energy $\mathbb{V}$. Once an INS exists, the wave function can only be distributed by the two sides, and thereby a specific mode of oscillation is induced. In this sense, although the QM cannot tell us exactly how the particles move, however, the mode of motion can be understood from the structure of the nodal surfaces. For example, 0(1) is dominated by a diamond with the D-SQ-D mode induced by the INS at SQ.

The preferred shapes and the associated modes of oscillation have been listed in Table I and Table II. The experimental observation of them is a great challenge to acquire a deeper understanding of the QM.

(2) This paper provides vivid examples of how each state pursues the best structure favorable to binding under the constraints of the QM symmetry and orthogonality. For example, 0(2) has to avoid the SQ because the $L=0$ states are SQ inaccessible, to avoid the diamond because the 0(1) state has possessed the diamond, among the inversion-invariant shapes, the rectangle is adopted; and accordingly a REC-SQ-REC mode is induced by the INS at SQ. One more example is the 2(2) state; it has to avoid the SQ because the 2(1) state has possessed the SQ; it is not very advantageous to possess an inversion-invariant shape because two nodal lines will be contained [Fig. 7(b)]; consequently, the 2(2) state is a mixture of an inversion-invariant shape and an inversion-variant shape.

(3) The discovery of the monopole excitation (breathing mode) in two-dimensional systems is noticeable. In nuclear theory, the monopole excitation is related to the incompressibility of the nuclear matter. A similar role may be played in quantum dots.

(4) The discovery of the CET structure is noticeable. There are two types of structures, namely, the centered structure (e.g., the CET) and the surface structure (e.g., the convex polygon). In four-electron dots, the centered structure is not favorable (hence, the CET emerges only in higher states). However, in five-electron dots, these two types of structure are nearly equal in competition. In six-electron dots, the centered structure may even overtake the surface structure. In seven or more electron dots, there may be more than one particle staying in the interior; thereby the interior structure begins to form, which has to match the surface structure.

(5) The existence of the magic angular momenta 2,6,10,... is noticeable. They stand out because all the other head states of spin-aligned systems are SQ inaccessible.

(6) From an analysis of the wave functions, the spectrum can be systematically understood. It was shown that the effect of QM symmetry is decisive. We can adjust the dynamical parameters to change the quantitative details, but the qualitative features remain unchanged. For example, when a state contains an INS at SQ [e.g., the 0(1) state], no matter how the parameters are adopted, the best choice is a diamond with the D-SQ-D mode. A group of states will pursue the same structure if they suffer the same constraints from the QM symmetry and orthogonality [e.g., the group 0(1),4(1),8(1)...; or the group 0(2),4(2),8(2)...] resulting in the existence of similarity. Based on the similarity, rotational bands are naturally formed. Since rotational bands are originated from QM symmetry, not only in quantum dots, they would widely exist in different few-body systems.

(7) Although only the $S=2$ states have been studied in detail, however, the $S=0$ and 1 states are also decisively determined by the QM symmetry.

In the $S=0$ states, the L even states are SQ accessible. Hence the 0(1),2(1),4(1),... states form a SQ band. The L odd states are SQ inaccessible; besides, they also cannot have inversion-invariant shapes (because in these shapes a rotation by 180° is equivalent to two interchanges of particles, the latter operation causes no effect in $S=0$ states). Consequently, the L odd head states are explicitly higher than the L even head states.

In the $S=1$ states, the 0(1),4(1),8(1),... form a SQ band with even parity; the 1(1), 3(1), 5(1),... form another SQ band with odd parity.

The formation of all these bands are determined by symmetry. Since the symmetry is global, not only certain states of the same system may be similar, the states of different systems (e.g., nuclear or atomic systems) also may have something in common.[15] This will lead to a unified understanding to different few-body systems.

ACKNOWLEDGMENTS

This work was supported by the National Natural Science Foundation of China and by the Guangdong Natural Science Foundation.

[1] T. Chakraborty, Comments Condens. Matter Phys. **16**, 35 (1992).
[2] B. Meurer, D. Heitman, and K. Ploog, Phys. Rev. Lett. **68**, 1371 (1992).
[3] R. C. Ashoori, H. L. Stormer, J. S. Weiner, L. N. Pfeiffer, K. W. Baldwin, and K. W. West, Phys. Rev. Lett. **71**, 613 (1993).
[4] R. B. Laughlin, Phys. Rev. B **27**, 3383 (1983).
[5] R. B. Laughlin, Phys. Rev. Lett. **50**, 1395 (1983).
[6] S. M. Girvin and Terrence Jach, Phys. Rev. B **28**, 4506 (1983).
[7] P. A. Maksym and T. Chakraborty, Phys. Rev. B **45**, 1947 (1992).
[8] P. Hawrylak and D. Phannkuche, Phys. Rev. Lett. **70**, 485 (1993).
[9] S-R Eric Yang, A. H. Macdonald, and M. D. Johnson, Phys. Rev. Lett. **71**, 3194 (1993).
[10] J. J. Palacios *et al.*, Phys. Rev. B **50**, 5760 (1994).
[11] W. Y. Ruan, Y. Y. Liu, C. G. Bao, and Z. Q. Zhang, Phys. Rev. B **51**, 7942 (1995).
[12] W. Y. Ruan, Y. Y. Liu, and C. G. Bao, J. Math. Phys. (to be published).
[13] I. Talmi, Helv. Phys. Acta **25**, 185 (1952).
[14] M. Moshinsky, Nucl. Phys. **13**, 104 (1959).
[15] C. G. Bao, Few-Body Syst. **13**, 41 (1992).
[16] W. Y. Ruan and C. G. Bao, Few-Body Syst. **14**, 25 (1993).
[17] C. G. Bao, Phys. Rev. A **47**, 1752 (1993).
[18] J. Avery, *Hyperspherical Harmonics, Application in Quantum Theory* (Kluwer, Dordrecht, 1989).
[19] C. G. Bao, W. F. Xie, and C. D. Lin, J. Phys. B **27**, L193 (1994).
[20] A. de Shalit and H. Feshbach, *Theoretical Nuclear Physics* (Wiley, New York, 1974).